

# Synthesis of SAPO-34 templated by diethylamine: Crystallization process and Si distribution in the crystals

Guangyu Liu<sup>a,b</sup>, Peng Tian<sup>a</sup>, Ying Zhang<sup>a,b</sup>, Jinzhe Li<sup>a,b</sup>, Lei Xu<sup>a</sup>,  
Shuanghe Meng<sup>a</sup>, Zhongmin Liu<sup>a,\*</sup>

<sup>a</sup> *Laboratory of Applied Catalysis, Dalian Institute of Chemical Physics, Chinese Academy of Sciences, 457 Zhongshan Road, Dalian 116023, PR China*

<sup>b</sup> *Graduate University of Chinese Academy of Sciences, Beijing 100049, PR China*

Received 27 September 2007; received in revised form 22 January 2008; accepted 24 January 2008

Available online 1 February 2008

## Abstract

The crystallization process of SAPO-34 molecular sieve with Si distribution in the crystals using diethylamine (DEA) as the template was investigated by XRD, SEM, IR, NMR, XRF, XPS and EDS techniques. It was found that the solution-mediated transport mechanism occurred during the crystallization, though the gel transformation cannot be completely excluded in the initial crystallization ( $t \leq 1$  h). Si directly participated in the crystallization in the initial stage and incorporated into the framework of SAPO-34 by SM2 (P substitution by Si) and SM3 (pairs of Al and P substitution by 2Si) mechanisms. XPS analysis revealed the enrichment of Si on the surface of crystals. Based on the experimental results, a model of Si distribution in the crystals was proposed, which described a non-uniform distribution of Si in the crystals, with the increasing content from the core to the surface.

© 2008 Elsevier Inc. All rights reserved.

**Keywords:** SAPO-34; Diethylamine; Characterization; Crystallization mechanism; Si distribution

## 1. Introduction

SAPO-34, a silicoaluminophosphate molecular sieve with CHA structure, has exhibited excellent catalytic performance in methanol-to-olefin (MTO) reaction due to the contribution of small pore, medium acidity and good thermal/hydrothermal stability [1–4]. In recent years, MTO reaction has been attracting much attention because it is the key step as a non-oil route to produce ethylene and propylene [4–11]. Accordingly, researches on SAPO-34 – the active composition of MTO catalyst, have also received considerable interests. Many efforts have been focused on understanding the reaction mechanisms [12–15] and improving the catalytic performance. However, the investigation on the synthesis and crystallization mechanism of

SAPO-34 is quite rare. As the catalytic performance of SAPO-34 is closely related to its acidic property and Si distribution, therefore, the detailed study on the synthesis mechanism would be helpful for controlling the framework composition and optimizing the acidic/catalytic property.

The crystallization of molecular sieves is a very complicated process influenced by reactants, mixing procedure, temperature, pH, etc. Two mechanisms regarding the crystallization process have been proposed [16–18]. One of which is the solution-mediated transport mechanism involving the dissolution of reagents followed by transport mechanisms to the nucleation sites where the crystal growth takes place, and the other is the solid hydrogel transformation mechanism involving the reorganization of the solid phase from amorphous components to crystalline. A combination of both mechanisms may also be possible; however, no general roles have hitherto been developed due to the complexity of crystallization process.

\* Corresponding author.

E-mail address: [liuzm@dicp.ac.cn](mailto:liuzm@dicp.ac.cn) (Z. Liu).

It is recognized that there exist two kinds of Si substitution mechanisms in the crystallization of SAPO molecular sieves [19–25]. One is the substitution of P by Si (denoted as SM2), which would form Si(4Al) entities and lead to the formation of negatively-charged frameworks (balanced by protons attached to Si–O–Al bridges). The other is the double substitution of adjacent P and Al by two Si atoms (denoted as SM3), which gives rise to Si(*n*Al) (*n* = 3 – 0) structures and stronger Brønsted acid sites.

Some attempts have been made to explore the crystallization from the mixture gel to SAPO-34. The crystallization of SAPO-34 using morpholine as the template in the presence of HF was studied by Vistad et al., who suggested that the gel first dissolves into 4-rings (4R) units, further constituting a layered intermediate (the prephase), and that the next steps are redissolution, nucleation and crystallization of the prephase in different types of 4R building units [26–28]. However, no direct information about Si substitution was obtained, since  $^{29}\text{Si}$  NMR was not applied in their studies. Therein, Si incorporation was proposed to proceed with the substitution of aluminum or phosphorus in the silicon-free 4R type-I units based on the elemental analysis results. Our group has reported the crystallization and Si incorporation mechanisms of SAPO-34 synthesized with triethylamine as the template [29], where the formation of SAPO-34 was possibly ascribed to the contribution of a gel conversion mechanism, with a two-stage crystallization process. In the first stage (less than 2.5 h), most of the crystallization (~80%) took place and the majority of Si (80%) incorporated into the framework of SAPO-34 by a direct insertion mechanism. In the second stage (longer than 2.5 h), the minority of Si (20%) inserted into the framework by the substitution of Si for P (SM2) as well as the substitution of 2Si for P + Al (SM3). Moreover, Huang et al. used cyclohexylamine as the template to investigate the synthesis of SAPO-44, which has the same structure as SAPO-34 but with different lattice symmetry [30]. They found that 2 h of hydrothermal treatment mainly generated an amorphous AlPO phase consisting of secondary building units, which would further assemble to half CHA cages, and that Si started to incorporate into the amorphous phase at later period. A layered material appeared after 6 h, and a further increase in heating time led to the formation of SAPO-44.

SAPO-34 can be synthesized with many templates, such as tetraethylammonium hydroxide (TEAOH) [1,10], dipropylamine [1], isopropylamine [1], piperidine [31], morpholine [20,26–28,32], triethylamine (TEA) [29,33] etc. However, only several investigations have involved in the synthesis of SAPO-34 templated by diethylamine (DEA) [34–37]. Our recent work indicated that DEA template could produce SAPO-34 with high purity and crystallinity [38]. Interestingly, the Si content of SAPO-34 synthesized with DEA was much higher than those with triethylamine (TEA) and tetraethylammonium hydroxide (TEAOH), even though the initial gel had similar compositions. The present paper reports detailed investigations on the crystal-

lization mechanism of SAPO-34 synthesized with DEA template, and on the Si distribution by employing XRD, SEM, IR, XRF, NMR, EDS and XPS techniques.

## 2. Experimental

### 2.1. Sample preparation

SAPO-34 was hydrothermally synthesized from the gel with a composition of 2.0DEA:0.6SiO<sub>2</sub>:1.0Al<sub>2</sub>O<sub>3</sub>:0.8-P<sub>2</sub>O<sub>5</sub>:50H<sub>2</sub>O. Pseudoboehmite, phosphoric acid (85 wt%) and silica sol (25 wt%) were used as the sources of aluminum, phosphorus and silicon, respectively. Pseudoboehmite was added to the diluted phosphoric acid solution, which was then stirred for 2 h until a uniform gel was obtained. To the resultant gel silica sol and DEA were successively added, and the stirring was maintained for 1 h to form a uniform reaction mixture, which was then sealed in a 2000 ml autoclave (Fig. 1) and heated from room temperature to 473 K at a rate of 2 K/min. The crystallization was carried out at 473 K under autogenous pressure while stirring. Samples were withdrawn periodically from the autoclave during the crystallization. The crystallization time was recorded once the temperature of autoclave had reached 473 K. As-synthesized samples were obtained after centrifugation, washing, and drying at 393 K for 4 h, in which some samples underwent calcination in air at 823 K for 5 h to remove the template and water. Solid yield experiments were performed separately in 200 ml autoclaves with the same gel composition as described above.

### 2.2. Characterizations

The powder XRD patterns of the samples were recorded on an X-ray diffractometer (Rigaku D/MAX-RB) with Cu K $\alpha$  radiation ( $\lambda = 0.15418$  nm). The crystal morphology was observed by scanning electron microscopy (KYKY-AMRAY-1000B). The chemical composition of the samples was determined with an X-ray fluorescence (XRF) spectrometer (Philips Magix-601), and those of some samples were also obtained by scanning electron microscope (JEOL-JSM-5600) equipped with an energy dispersive X-ray spectrometer (EDS, Oxford Link-ISIS-300). FT-IR spectra were measured using KBr-diluted pellet on an IR

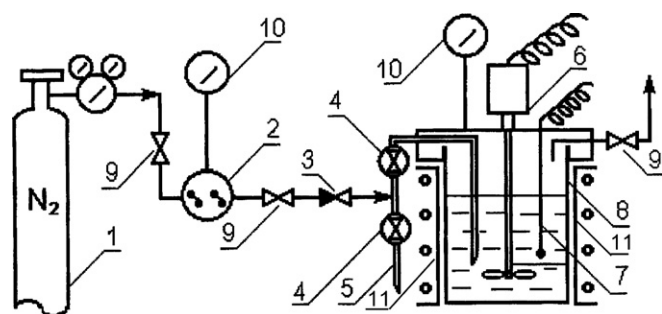


Fig. 1. Schematic diagram of the apparatus for SAPO-34 synthesis.

spectrophotometer (Bruker Tensor-27) at a resolution of  $4\text{ cm}^{-1}$ .  $^{29}\text{Si}$ ,  $^{27}\text{Al}$  and  $^{31}\text{P}$  MAS NMR spectral measurements were conducted on a Varian Infinity plus 400 WB spectrometer at resonance frequencies of 79.41, 104.17 and 161.83 MHz, respectively. The spinning rates of the samples at the magic angle were 4, 10 and 10 kHz for  $^{29}\text{Si}$ ,  $^{27}\text{Al}$  and  $^{31}\text{P}$ , respectively. The reference materials for the chemical shift (in ppm) were 2,2-dimethyl-2-silapentane-5-sulfonate sodium salt (DSS) for  $^{29}\text{Si}$ , 1 mol/l  $\text{Al}(\text{H}_2\text{O})_6^{3+}$  for  $^{27}\text{Al}$  and 85%  $\text{H}_3\text{PO}_4$  for  $^{31}\text{P}$ . XPS measurements were performed on a VG ESCALAB MKII spectrometer using Al  $K\alpha$  radiation (1486.6 eV) as the excitation source. Quantitative analysis of atomic ratios was obtained by determining the elemental areas of the core-level peaks O 1s, Si 2p, Al 2p and P 2p.

### 3. Results and discussion

#### 3.1. Crystallization process

##### 3.1.1. XRD and SEM

The powder XRD patterns of as-synthesized samples with different crystallization time are shown in Fig. 2. During the whole crystallization process, SAPO-34 was detected as the only crystalline phase. At  $t = 0\text{ h}$  (just when the crystallization temperature reached 473 K), the XRD pattern of the solid sample was mainly consisted of amorphous boehmite; however, very weak peaks emerged at  $9.4^\circ$  and  $20.6^\circ$ , suggesting the appearance of very small amount of SAPO-34 crystals. This implies fast crystallization characteristic of SAPO-34 under given conditions. The diffrac-

tion peaks of SAPO-34 became evident after 0.5 h of crystallization time and the intensity of peaks was greatly enhanced with time. The crystallization curve on the basis of relative crystallinity is given in Fig. 3. During the initial 4 h, the relative crystallinity increased sharply with time and reached 90% at  $t = 4\text{ h}$ . Later on, the high crystallinity of SAPO-34 was kept almost unchanged.

Fig. 4 presents SEM images of as-synthesized samples. Only an amorphous phase existed at 0 h. After 0.5 h, small amount of cubic-like rhombohedra crystals (typical of SAPO-34 morphology) was observed. Further increasing the crystallization time to 4 h led to a fast transformation of crystalline phase. Upon heating the gel for 10 h or longer, amorphous phase was totally invisible and only crystals were observed. Generally, SAPO-34 crystals grew larger and larger with the process of crystallization.

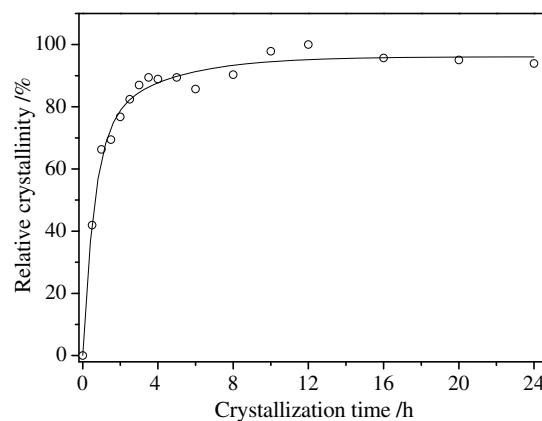


Fig. 3. Crystallization curve of SAPO-34.

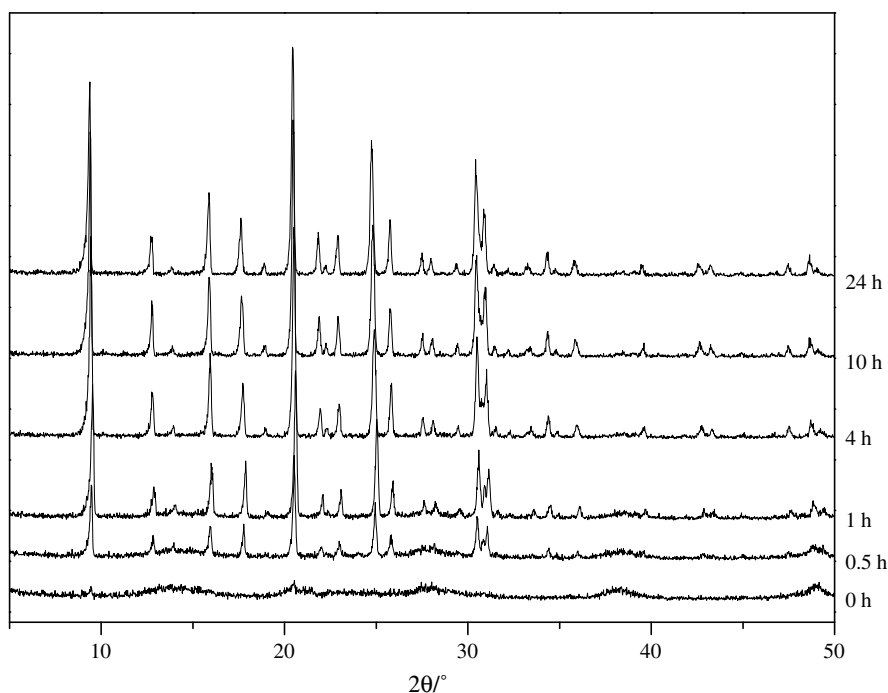


Fig. 2. XRD patterns of as-synthesized samples with different crystallization time.

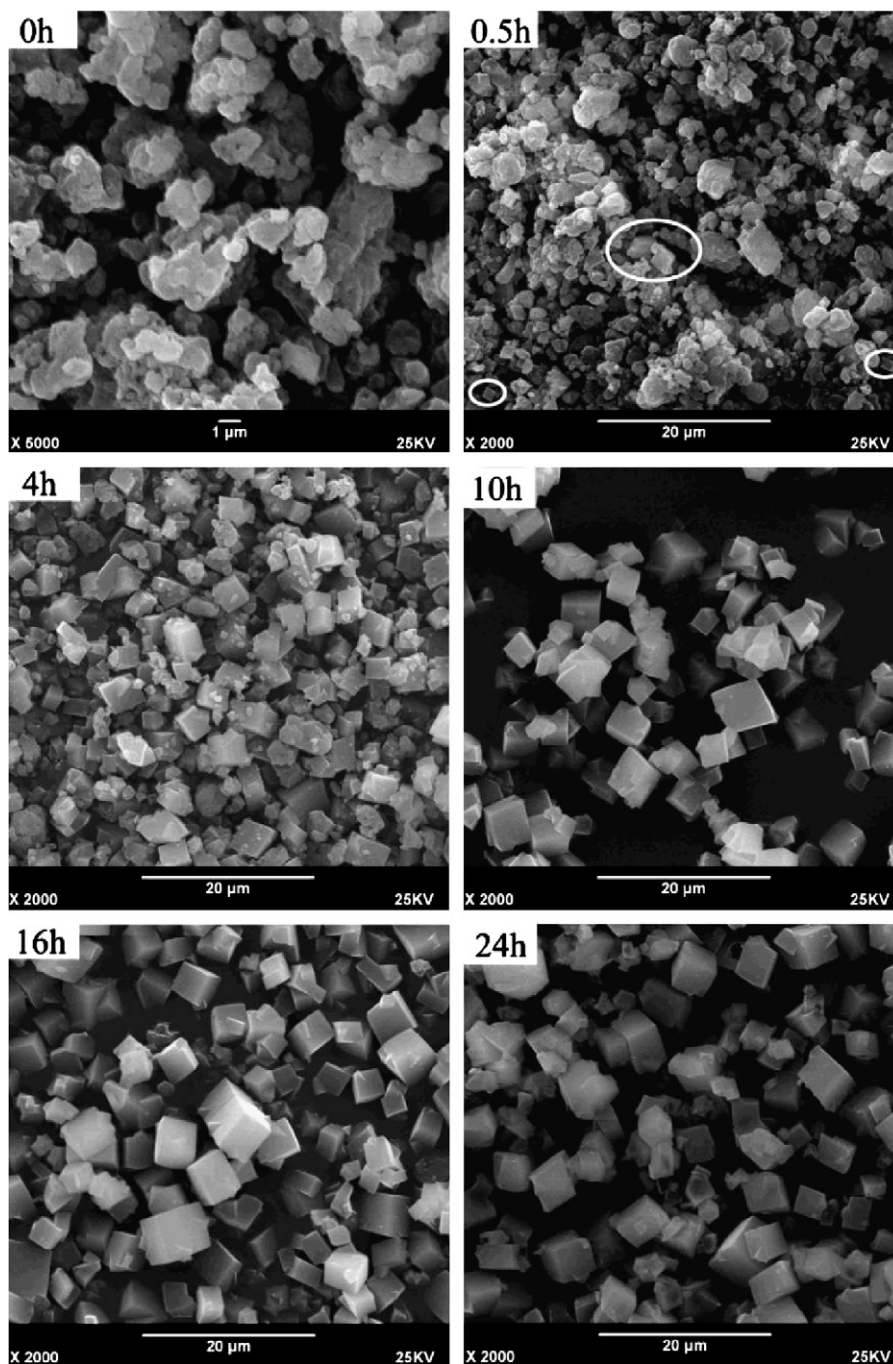


Fig. 4. SEM images of as-synthesized samples.

### 3.1.2. FT-IR Spectra

Fig. 5 shows FT-IR spectra of as-synthesized samples. According to the literature [23,29,39], all peaks are assigned as follows:  $3650\text{--}3000\text{ cm}^{-1}$  arising from the hydroxyl vibration;  $1300\text{--}1000\text{ cm}^{-1}$  ascribed to the asymmetric stretch of T-O tetrahedra;  $740\text{ cm}^{-1}$  due to the symmetric stretch of T-O tetrahedra; the peaks below  $700\text{ cm}^{-1}$  corresponding to the vibration of double-6 rings and the bending of T-O.

The broad triplet between  $1000$  and  $400\text{ cm}^{-1}$  and the strong broad peaks between  $3650$  and  $3000\text{ cm}^{-1}$  in the spectrum at  $t = 0\text{ h}$  indicate the amorphous characteristic

of the sample. After  $0.5\text{ h}$ , the peaks in the spectra became sharp with typical characteristics of molecular sieves. When the crystallization time was longer than  $0.5\text{ h}$ , all of the IR spectra were almost similar except the peak intensity in the range of  $1500\text{--}400\text{ cm}^{-1}$  kept a rise with time, suggesting the increase of crystallinity and the gradual incorporation of the template (the band at  $1480\text{ cm}^{-1}$ ) into the crystals. Moreover, the peaks in the range of  $3000\text{--}3650\text{ cm}^{-1}$  weakened obviously with time, indicating the condensation of hydroxyl groups. These changes were in agreement with the results of XRD and SEM.

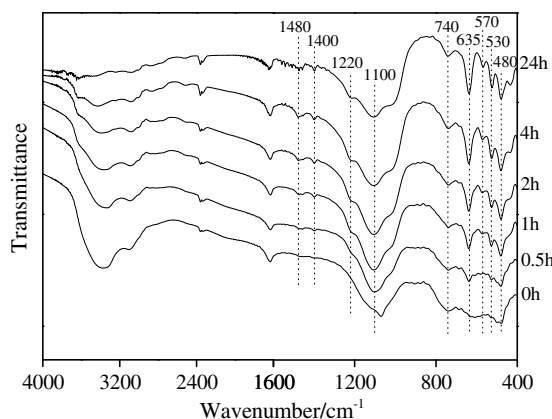
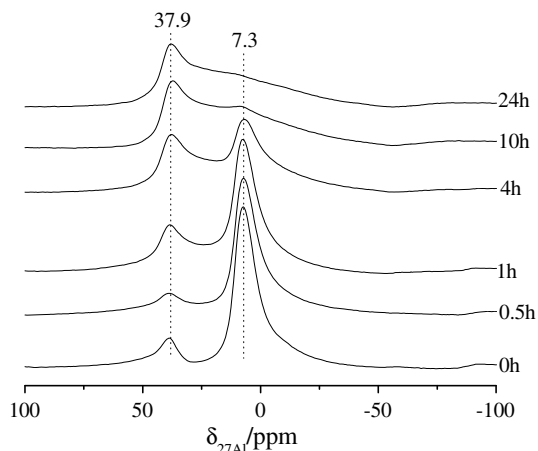
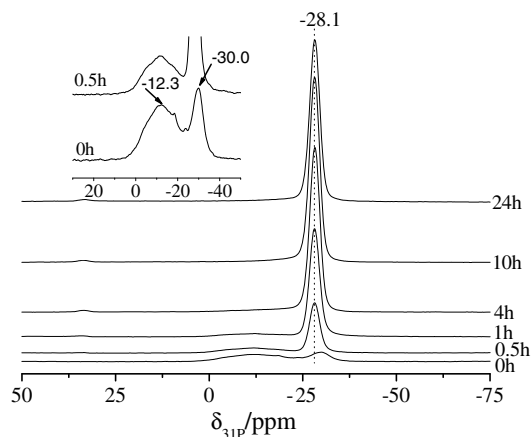


Fig. 5. FT-IR spectra of as-synthesized samples.

### 3.1.3. MAS NMR spectra

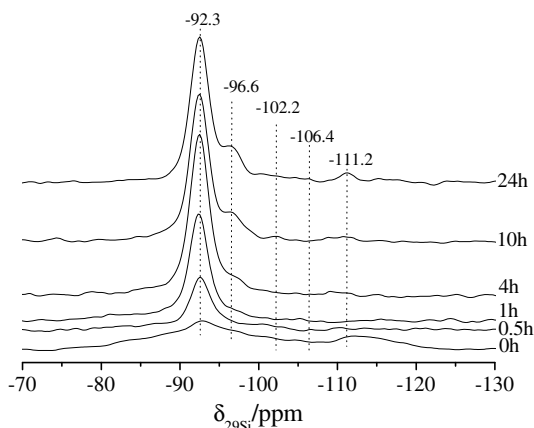
$^{27}\text{Al}$  MAS NMR spectra of as-synthesized samples are shown in Fig. 6. The spectrum of the sample at  $t = 0$  h exhibits a weak peak at 37.9 ppm and a strong one at 7.3 ppm. With the increase of crystallization time, the former peak became intense and the latter weakened gradually but was still visible even after 24 h. The peak at 37.9 ppm is due to Al in tetrahedral environments in the framework [23,39,40], indicating that tetrahedral Al sites were present already at  $t = 0$  h. However, the ascription of the peak at 7.3 ppm is equivocal. Both five-coordinated Al sites in the framework [40] and amorphous alumina source [29,30] may give rise to a resonance peak around 7 ppm. Considering the results of XRD, SEM and IR, the strong peak at 7.3 ppm could mainly arise from amorphous alumina source at the crystallization period of  $t \leq 4$  h. Afterwards, with the increase of crystals and the dissolution of amorphous alumina into the liquid phase, the peak at 7.3 ppm was mainly contributed by five-coordinated Al in the framework of SAPO-34, especially for the samples of  $t \geq 10$  h.

Fig. 7 presents  $^{31}\text{P}$  MAS NMR spectra of as-synthesized samples. At  $t = 0$  h, there are a relatively sharp peak at

Fig. 6.  $^{27}\text{Al}$  MAS NMR spectra of as-synthesized samples.Fig. 7.  $^{31}\text{P}$  MAS NMR spectra of as-synthesized samples.

–30.0 ppm, arising from  $\text{P}(\text{OAl})_4$  species, and a broad peak around –12.3 ppm, assigned to the P sites in the amorphous material [29,30]. The former peak shifted from –30.0 ppm to –28.1 ppm and was evidently strengthened at 0.5 h. The signal due to amorphous P disappeared when  $t > 1$  h, indicating that P species generating SAPO-34 crystals came from the liquid phase.

As shown in Fig. 8,  $^{29}\text{Si}$  MAS NMR spectrum of sample at  $t = 0$  h exhibits two peaks centered at –112.1 ppm (weak) and –92.3 ppm (broad), resulting from tetrahedral Si in amorphous silica [30] and from isolated  $\text{Si}(\text{OAl})_4$  species in the SAPO structure, respectively. However, Si species from Si–Al domains may exist as well and contribute to notable broadness of the peak at –92.3 ppm [41]. At  $t = 0.5$  h, the peak at –92.3 ppm became sharper but the other at –112.1 ppm disappeared, suggesting the dissolution of amorphous silica and Si–Al domains. At  $t = 4$  h, two weak peaks emerged at –96.6 ppm and –111.2 ppm, which are ascribed to  $\text{Si}(\text{OAl})_3(\text{OSi})$  and  $\text{Si}(\text{OSi})_4$ , respectively. The appearance of  $\text{Si}(\text{OAl})_3(\text{OSi})$  and  $\text{Si}(\text{OSi})_4$  species is in agreement with the Si environments of 5Si islands [22,29], implying the substitution of Si for P (SM2) and the pairs of P and Al (SM3). When  $t = 10$  h,

Fig. 8.  $^{29}\text{Si}$  MAS NMR spectra of as-synthesized samples.

a new weak signal due to  $\text{Si}(\text{OAl})_2(\text{OSi})_2$  appeared at  $-102.2$  ppm, which suggests the generation of 8Si or even larger islands. At the end of crystallization ( $t = 24$  h), all of five Si peaks could be observed simultaneously.

### 3.1.4. Elemental analysis

The chemical compositions of samples obtained by XRF are presented in Fig. 9. Only Al, P and Si elements were detected. The content of Al in the samples was always higher than those of P and Si during the crystallization process. The contents of P and Si in the samples increased but that of Al decreased rapidly before 4 h, indicating that the amorphous materials observed by SEM at the early crystallization period should be mainly from unreacted alumina, which dissolved gradually into the liquid phase with time. After 10 h the solid compositions were maintained roughly unchanged. Thus, the XRF compositions of the samples were directly related to the bulk composition of SAPO-34 during the period of 10–24 h.

### 3.1.5. Solid yield

The relative solid yield as a function of the crystallization time is described in Fig. 10. Before 2 h, the relative solid yields were low and did not vary too much. Since the elemental composition in the solid at the early stage changed fast (Fig. 9), so the little change in solid yields should be resulted from the counteraction between the dissolution of amorphous alumina into the solution and the generation of crystals. A fast increase of the yield was observed during the period from 2 to 10 h. After 10 h, the yield still increased but with a much flatter slope.

## 3.2. Crystallization mechanism

At the initial crystallization stage ( $t \leq 1$  h), the solid products were composed of amorphous oxides (Si, P and Al) and small amount of SAPO-34, as evidenced by NMR, SEM and XRF results. After 1 h, no amorphous

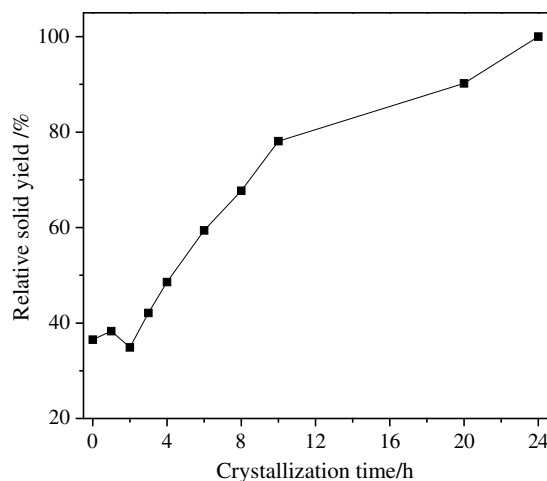


Fig. 10. Relative solid yield of as-synthesized samples.

Si and P existed in the solid (based on NMR results); only unreacted alumina was left as the amorphous residue. After 10 h, all of amorphous phases were transformed into pure crystals.

Based on the above results and the gradual incorporation of organic template into the solid products (FT-IR results), it is suggested that the solution-mediated transport mechanism occurred during the crystallization of SAPO-34, while the gel transformation could have happened in the initial crystallization ( $t \leq 1$  h).

### 3.2.1. Si incorporation mechanism

The results of  $^{27}\text{Al}$ ,  $^{31}\text{P}$  and  $^{29}\text{Si}$  MAS NMR spectra suggest that the preliminary structure units similar to the framework of SAPO-34 have been built at the beginning of crystallization ( $t = 0$  h), and that direct incorporation of Si into the framework of SAPO-34 may have happened in the initial stage. The sequent substitution of Si for P and then for the pairs of P and Al would occur in the latter

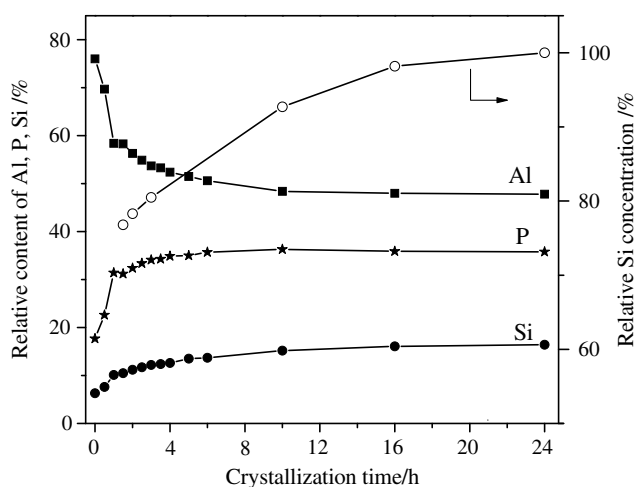


Fig. 9. Chemical composition of as-synthesized samples and relative Si concentration in SAPO-34.

Table 1

Elemental compositions obtained from XRF, XPS and SEM-EDS analysis

Samples		Elemental composition (mol%)		
		Al	Si	P
XRF	$t = 10$ h	48.4	15.2	36.3
	$t = 24$ h	47.8	16.4	35.8
XPS	$t = 24$ h	44.0	23.1	32.9
EDS*	$t = 4$ h	32.7	17.0	50.3
		30.9	16.9	52.2
		32.4	16.3	51.3
	$t = 10$ h	29.6	17.5	52.9
		29.4	18.9	51.7
		29.4	17.6	53.0
	$t = 24$ h	28.6	19.9	51.5
		29.4	20.0	50.6
		28.7	21.0	50.3

\* Data of samples at each crystallization time were obtained from randomly selected three crystals.

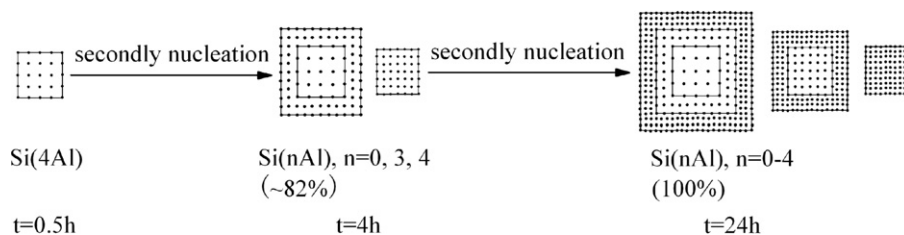


Fig. 11. Schematic diagram of crystallization process with Si distribution in the crystals.

stage. It is similar to the crystallization process of SAPO-34 templated by triethylamine [29], though SAPO-34 synthesized with DEA template showed higher Si insertion [38].

### 3.3. Si distribution in the crystals

The relation of Si concentrations in SAPO-34 crystals to the crystallization time, defined as  $(n_{\text{Si}}/n_{\text{Si+Al+P}})_t / (n_{\text{Si}}/n_{\text{Si+Al+P}})_{24\text{h}}$ , is depicted in Fig. 9. The values before 3 h were roughly calculated by assuming the existence of only Si(4Al) environment in the crystal in order to eliminate the influence of amorphous  $\text{Al}_2\text{O}_3$  in the samples. 76.8% of Si has been incorporated into the crystal at  $t = 1.5$  h, which then increased with time to reach 100% at  $t = 24$  h. The feasible reasoning could be that with the consumption of reactants and the production of SAPO-34 during the synthesis, the pH value of the mixture increased gradually [42], which would exert an impact on the polymerization degree of colloidal silica, and thus promote the incorporation degree of Si into the framework.

XPS experiment was carried out to obtain the information of the surface composition of SAPO-34 crystals (shown in Table 1). It was found that the Si content on the surface is higher than that in the bulk, indicating the Si enrichment phenomenon on the surface of crystals. The similar phenomena were also observed for the synthesis of other SAPO molecular sieves, such as SAPO-5 [43], SAPO-11, SAPO-31 [44] and SAPO-44 [45].

SEM-EDS results are shown in Table 1. Though EDS analysis can not give the quantitative result, it clearly shows the increase of the Si content on the surface of SAPO-34 with time. The Si contents on different crystals of one sample are close, suggesting the homogeneity of crystal surface composition.

The increase of Si content in SAPO-34 crystals and solid yields with the crystallization time suggests that the Si distribution in the crystals is possibly not uniform. In combination with the XPS and EDS results, a model regarding the Si distribution in the crystals was proposed and shown in Fig. 11. Since the properties of the mixture solution (pH value, reactant species and concentrations) always changed during the growth of crystals, therefore, the composition of newly grown layer on one crystal would be different from that of the original layer. Thus, the non-uniformity of Si concentration in the crystals shows a gradual increase of the Si content from the core to the surface. Meanwhile,

the increase of solid yields and the heterogeneity of crystal sizes shown by SEM revealed the occurrence of secondly nucleation during the crystallization process.

## 4. Conclusions

The crystallization process of SAPO-34 templated by DEA was investigated in detail. The solution-mediated transport mechanism occurred during the crystallization, but the gel transformation could also happen in the initial crystallization ( $t \leq 1$  h). Si incorporation mechanism in the present work was the same as that of SAPO-34 synthesized with TEA as the template and SM2/SM3 substitution mechanisms occurred during the crystallization. The Si concentration in SAPO-34 crystals increased with the crystallization time and there was a Si enrichment phenomenon on the crystal surface. A model of Si distribution in the crystals was proposed, which described a non-uniform distribution of Si in the crystals, with the increasing content from the core to the surface. Moreover, solid yield experiments and SEM images confirmed the existence of secondly nucleation during the crystallization process.

## References

- [1] B.M. Lok, C.A. Messina, R.L. Patton, R.T. Gajek, T.R. Cannan, E.M. Flanigen, US Patent 4440871, 1984.
- [2] J. Liang, H.Y. Li, S.Q. Zhao, W.G. Guo, R.H. Wang, M.L. Ying, Appl. Catal. 64 (1990) 31.
- [3] M. Stöcker, Micropor. Mesopor. Mater. 29 (1999) 3.
- [4] X.C. Wu, M.G. Abraha, R.G. Anthony, Appl. Catal. A 260 (2004) 63.
- [5] J.Q. Chen, A. Bozzano, B. Glover, T. Fuglerud, S. Kvisle, Catal. Today 106 (2005) 103.
- [6] D.R. Dubois, D.L. Obrzut, J. Liu, J. Thundimadathil, P.M. Adekanattu, J.A. Guin, A. Punnoose, M.S. Seehra, Fuel Process. Technol. 83 (2003) 203.
- [7] W.G. Song, H. Fu, J.F. Haw, J. Am. Chem. Soc. 123 (2001) 4749.
- [8] M. Kang, J. Mol. Catal. A 160 (2000) 437.
- [9] D. Chen, K. Moljord, T. Fuglerud, A. Holmen, Micropor. Mesopor. Mater. 29 (1999) 191.
- [10] S. Wilson, P. Barger, Micropor. Mesopor. Mater. 29 (1999) 117.
- [11] M. Popova, C. Minchev, V. Kanazirev, Appl. Catal. A 169 (1998) 227.
- [12] Z.M. Cui, Q. Liu, W.G. Song, L.J. Wan, Angew. Chem. Int. Ed. 45 (2006) 6512.
- [13] M. Hunger, M. Seiler, A. Buchholz, Catal. Lett. 74 (2001) 61.
- [14] W.G. Song, J.F. Haw, J.B. Nicholas, C.S. Heneghan, J. Am. Chem. Soc. 122 (2000) 10726.
- [15] B. Arstad, S. Kolboe, J. Am. Chem. Soc. 123 (2001) 8137.
- [16] R.J. Francis, D. O'Hare, J. Chem. Soc., Dalton Trans. (1998) 3133.

- [17] D. Uzcátegui, G. González, *Catal. Today* 107–108 (2005) 901.
- [18] C.S. Cundy, P.A. Cox, *Micropor. Mesopor. Mater.* 82 (2005) 1.
- [19] G. Sastre, D.W. Lewis, C.R.A. Catlow, *J. Phys. Chem.* 100 (1996) 6722.
- [20] G. Sastre, D.W. Lewis, C.R.A. Catlow, *J. Phys. Chem. B* 101 (1997) 5249.
- [21] G. Sastre, D.W. Lewis, C.R.A. Catlow, *J. Mol. Catal. A* 119 (1997) 349.
- [22] D. Barthomeuf, *Zeolites* 14 (1994) 394.
- [23] A.M. Prakash, S. Unnikrishnan, *J. Chem. Soc., Faraday Trans.* 90 (1994) 2291.
- [24] E.M. Flanigen, R.L. Patton, S.T. Wilson, in: P.J. Grobet, W.J. Mortier, E.F. Vansant, G. Schulz-Ekloff (Eds.), *Innovation in Zeolite Materials Science, Studies in Surface Science and Catalysis*, Vol. 37, Elsevier, Amsterdam, 1988, p. 13.
- [25] H.O. Pastore, S. Coluccia, L. Marchese, *Ann. Rev. Mater. Res.* 35 (2005) 351.
- [26] Ø.B. Vistad, E.W. Hansen, D.E. Akporiaye, K.P. Lillerud, *J. Phys. Chem. A* 103 (1999) 2540.
- [27] Ø.B. Vistad, D.E. Akporiaye, K.P. Lillerud, *J. Phys. Chem. B* 105 (2001) 12437.
- [28] Ø.B. Vistad, D.E. Akporiaye, F. Taulelle, K.P. Lillerud, *Chem. Mater.* 15 (2003) 1639.
- [29] J. Tan, Z.M. Liu, X.H. Bao, X.C. Liu, X.W. Han, C.Q. He, R.S. Zhai, *Micropor. Mesopor. Mater.* 53 (2002) 97.
- [30] Y. Huang, D. Machado, C.W. Kirby, *J. Phys. Chem. B* 108 (2004) 1855.
- [31] E. Dumitriu, A. Azzouz, V. Hulea, D. Lutic, H. Kessler, *Microporous Mater.* 10 (1997) 1.
- [32] L. Marchese, A. Frache, E. Gianotti, G. Martra, M. Causa, S. Coluccia, *Micropor. Mesopor. Mater.* 30 (1999) 145.
- [33] Y.X. Wei, D.Z. Zhang, Z.M. Liu, B.L. Su, *J. Catal.* 238 (2006) 46.
- [34] C.Q. He, Z.M. Liu, G.Y. Cai, L.X. Yang, Z.Z. Wang, J.S. Luo, X.S. Pan, Z.Q. Ge, Y.J. Chang, R.M. Shi, CN Patent 1096496, 1994.
- [35] Y.Y. Zheng, T.L. Yang, X.H. Zhou, S.K. Shen, *J. Fuel Chem. Technol.* 27 (1999) 139.
- [36] J. Li, F.M. Zhang, L.S. Li, X.T. Shu, *Petrol. Process. Petrochem.* 36 (2005) 49.
- [37] L.J. Wang, L.L. Xie, H. Yuan, Q.H. Li, Q.Z. Li, *Acta Chim. Sinica* 65 (2007) 170.
- [38] G.Y. Liu, P. Tian, J.Z. Li, D.Z. Zhang, F. Zhou, Z.M. Liu, *Micropor. Mesopor. Mater.* (2007), doi:10.1016/j.micromeso.2007.07.023.
- [39] S. Ashtekar, S.V.V. Chilukuri, D.K. Chakrabarty, *J. Phys. Chem.* 98 (1994) 4878.
- [40] A. Buchholz, W. Wang, M. Xu, A. Arnold, M. Hunger, *Micropor. Mesopor. Mater.* 56 (2002) 267.
- [41] M. Briend, R. Vomscheid, M.J. Peltre, P.P. Man, D. Barthomeuf, *J. Phys. Chem.* 99 (1995) 8270.
- [42] Ø.B. Vistad, D.E. Akporiaye, F. Taulelle, K.P. Lillerud, *Chem. Mater.* 15 (2003) 1650.
- [43] S.A. Schunk, D.G. Demuth, B. SchulzDobrick, K.K. Unger, F. Schuth, *Microporous Mater.* 6 (1996) 273.
- [44] A.K. Sinha, S. Seelan, *Appl. Catal. A* 270 (2004) 245.
- [45] D.B. Akolekar, S.K. Bhargava, J. Gorman, P. Paterson, *Colloids Surf., A* 146 (1999) 375.